ORNL/TM-2022/2721

Status of Additive Manufacturing Capabilities for Processing Refractory Alloys Under the Molybdemum-99 Program

Holden C. Hyer

Approved for public release.
Distribution is unlimited.

October 2022

OAK RIDGE National Laboratory

ORNL IS MANAGED BY UT-BATTELLE LLC FOR THE US DEPARTMENT OF ENERGY
Approved for public release.

DOCUMENT AVAILABILITY

Reports produced after January 1, 1996, are generally available free via OSTI.GOV.

Website www.osti.gov

Reports produced before January 1, 1996, may be purchased by members of the public from the following source:

National Technical Information Service
5285 Port Royal Road
Springfield, VA 22161
Telephone 703-605-6000 (1-800-553-6847)
TDD 703-487-4639
Fax 703-605-6900
E-mail info@ntis.gov
Website http://classic.ntis.gov/

Reports are available to US Department of Energy (DOE) employees, DOE contractors, Energy Technology Data Exchange representatives, and International Nuclear Information System representatives from the following source:

Office of Scientific and Technical Information
PO Box 62
Oak Ridge, TN 37831
Telephone 865-576-8401
Fax 865-576-5728
E-mail reports@osti.gov
Website https://www.osti.gov/

This report was prepared as an account of work sponsored by an agency of the United States Government. Neither the United States Government nor any agency thereof, nor any of their employees, makes any warranty, express or implied, or assumes any legal liability or responsibility for the accuracy, completeness, or usefulness of any information, apparatus, product, or process disclosed, or represents that its use would not infringe privately owned rights. Reference herein to any specific commercial product, process, or service by trade name, trademark, manufacturer, or otherwise, does not necessarily constitute or imply its endorsement, recommendation, or favoring by the United States Government or any agency thereof. The views and opinions of authors expressed herein do not necessarily state or reflect those of the United States Government or any agency thereof.

ORNL/TM-2022/2721

Nuclear Energy and Fuel Cycle Division

STATUS OF ADDITIVE MANUFACTURING CAPABILITIES FOR PROCESSING REFRACTORY ALLOYS UNDER THE MOLYBDENUM-99 PROGRAM

Holden C. Hyer

October 2022

Prepared by
OAK RIDGE NATIONAL LABORATORY
Oak Ridge, TN 37831
managed by
UT-BATTELLE LLC
for the
US DEPARTMENT OF ENERGY
under contract DE-AC05-00OR22725

CONTENTS

CONTENTS iii
LIST OF FIGURES iv
ACKNOWELDGMENTS v
ABSTRACT 6
1. BACKGROUND 7
   1.1 MOLYBDENUM-99 ACCELERATOR PRODUCTION 7
   1.2 ADDITIVE MANUFACTURING 7
2. EXPERIMENTAL FACILTIES 9
   2.1 POWDER PRODUCTION 9
   2.2 LASER POWDER BED FUSION 12
   2.3 MATERIALS CHARACTERIZATION 15
3. LASER POWDER BED FUSION PROCESSING OF REFRACTORY ALLOYS 17
4. SUMMARY 20
5. REFERENCES 21

LIST OF FIGURES

Figure 1. Schematic of the LPBF process. 8
Figure 2. SEM images of (a) as-received, (b) spray-dried, and (c) plasma-spherodized pure Mo powder. 10
Figure 3. (a) The Niro spray dryer and (b) Tekna plasma spherodization systems located at ORNL. 12
Figure 4. The (a) Renishaw AM250 LPBF system and its (b) RBV setup installed in the build chamber; (c) Different geometries printed from pure Mo powder based on design work from the Molybdenum-99 Program. 13
Figure 5. Examples of processing parametric studies performed by (a) printing simple cubic geometries in which (b) the LPBF parameters can be easily varied between each cube. 15
Figure 6. Characterization equipment includes (a) the Malvern Panalytical particle analyzer and (b) the UES Robo-Met serial sectioning unit. 16
Figure 7. Density as a function of ED for pure Mo printed at low (200 W) and high (400 W) laser power. 18
Figure 8. Optical image of the cross section of a Mo sample with respect to the build direction. 19

ACKNOWELDGMENTS

Support for this work was provided by the US Department of Energy's National Nuclear Security Administration, Office of Material Management and Minimization's Molybdenum-99 Program.

ABSTRACT

The enriched ^{100}Mo target, denoted as *aMo*, that Northstar Medical Radioisotopes is developing to produce ^{99}Mo from an accelerator-based method is a disk-type geometry with a 0.5–0.715 mm thickness and a 29 mm outer diameter. A press and sinter method was adopted to fabricate these samples from aMo powder feedstock. Inherent porosity from the press and sinter method makes the disks more easily dissolvable during ^{99}Mo postprocessing. However, the disk-type geometry will be subject to thermal stresses due to temperature variations once the geometry is in line with the accelerated electron beam, causing warping and possible failure. Additive manufacturing (AM) processes such as laser powder bed fusion (LPBF) enable the manufacturing of custom, complex geometries that may otherwise be difficult to produce with more conventional methods (e.g., press and sinter approach). Therefore, the National Nuclear Security Administration's Molybdenum-99 Program invested in developing an AM facility dedicated to processing and printing refractory powders. This report details the LPBF process, how irregular refractory powder can be prepared for LPBF, and the equipment that is available to support the program.

1. BACKGROUND

1.1 MOLYBDENUM-99 ACCELERATOR PRODUCTION

Northstar Medical Radioisotopes (hereafter referred to as *Northstar*) is developing an accelerator-based method for producing ^{99}Mo, a parent isotope of ^{99m}Tc. ^{99m}Tc is used for medical imaging purposes. An enriched ^{100}Mo target, denoted as *aMo*, can be synthesized with a typical enriched U fission reactor. aMo is a stable isotope of Mo and is not radioactive. To remove a neutron from the aMo atom and reduce it to ^{99}Mo, the targets will be directed inline of an accelerated electron beam. The current geometry of the target is a 29 mm diameter disk with a thickness of 0.5–0.715 mm. aMo and any other Mo isotope, including pure ^{nat}Mo, starts as a powder feedstock because of Mo's high melting temperature (~2600 °C). As a result, a press and sinter method was adopted to manufacture the aMo targets. Through the funding provided by the National Nuclear Security Administration (NNSA), Oak Ridge National Laboratory (ORNL) helped developed and fabricate aMo targets for Northstar.

Previous work was performed to optimize the press and sinter method by evaluating different pressing pressures and sinter times using pure Mo powder as a surrogate, as documented in previous reports [1]. The press and sinter method results in inherent porosity that is difficult to minimize without subsequent working, such as hot rolling or extrusion, typically performed to manufacture dense ^{nat}Mo into a wrought form. Dissolution of the target postexposure will be performed in an acidic media, such as peroxide, which can then subsequently be used in the generators used to make ^{99m}Tc. Any additional surface area created by the pores or voids in the target accelerates the time to dissolution [2, 3]. However, these pores or voids could hinder mechanical performance.

Exposing the disk to the accelerator will cause high-temperature gradients throughout the disk. These disks will be grouped in stacks of 60 and exposed to the accelerator for up to 6 days [4, 5]. Helium will be used as a coolant and jetted in between the front and back face of disk. The center of the disk where the electron beam will be focused is expected to reach ~1000 °C, hundreds of degrees hotter than near the edges of the disk. Therefore, the disk could warp, which could cause target failure and possibly cascading failure throughout the 60 disk stack [6, 7]. As an alternative to the press and sinter method, advanced manufacturing techniques such as additive manufacturing (AM) can be used to design a target geometry with an optimized shape that can withstand the thermal environment and any mechanical stresses [8]. Moreover, AM can be used to engineer porosity for increased dissolution, similar to what is expected from the press and sinter approach. This report details the AM capabilities at ORNL as part of an NNSA investment to fabricate ^{nat}Mo and aMo disks from feedstock powder.

1.2 ADDITIVE MANUFACTURING

Most metal AM processes are performed layer by layer, meaning that material is locally deposited, melted, or welding together in a repetitive process to form a part [9]. The most common AM methods include melting strategies, such as powder bed fusion (PBF) and direct energy deposition (DED) [9]. PBF is commonly used because it is relatively easy to perform. PBF also generally has better geometric resolution than DED because PBF can handle smaller particle sizes of <50 µm, whereas DED requires larger powder sizes of >50–300 µm [9]. In PBF, a powder bed is selectively melted by either an electron beam or laser source. Electron-beam PBF can fabricate components faster, but the surface quality is often not adequate and requires postprocessing to clean the surface. Laser PBF (LPBF) is slower, but the surface roughness on parts is much finer and can be reduced to only a few microns. LPBF has been used to process a wide variety of materials, including stainless steels, Ni-based superalloys, Al alloys, Mg alloys, and even Mo alloys [9-13].

Figure 1 provides a schematic of a typical LPBF process. Powder is fed into the system—in this case, through a powder well—and a wiper is used to push and spread the powder over the build plate; the build plate is used as the starting substrate. The build plate is mounted on an elevator platform that will continually move down incrementally during the build, holding the part and the powder bed in the elevator shaft. After each subsequent laser scan, the build platform will move down, new powder will be raked across, and the process will continue until the build is done. The elevator can then be returned to the top, the powder recycled, and the component extracted from the build chamber.

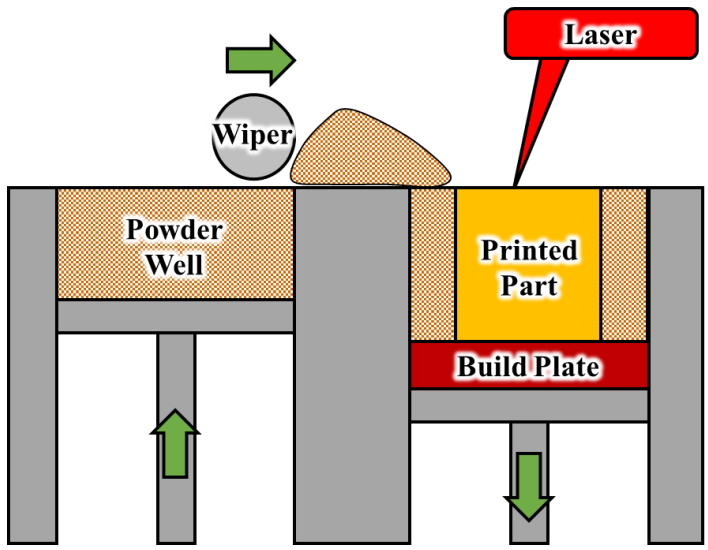

Figure 1. Schematic of the LPBF process.

2. EXPERIMENTAL FACILTIES

2.1 POWDER PRODUCTION

Molybdenum is typically processed from a powder form because of its high melting temperature, which makes it attractive for powder-based AM methods such as LPBF. To break down larger pieces or ingots, Mo is often subjected to milling operations that create a powder with irregular geometries, as shown in Figure 2(a). For press and sinter methods or hot rolling operations, the irregular powder geometry may assist in compaction and thus may not be a concern for these processes. However, irregular powder is often not free flowing, which is critical for LPBF. Moreover, irregular particles may not melt effectively during the local melting of LPBF, which could cause large voids or pores to form during a component build. Spherical powder provides the best flowability and enables a more uniform melting.

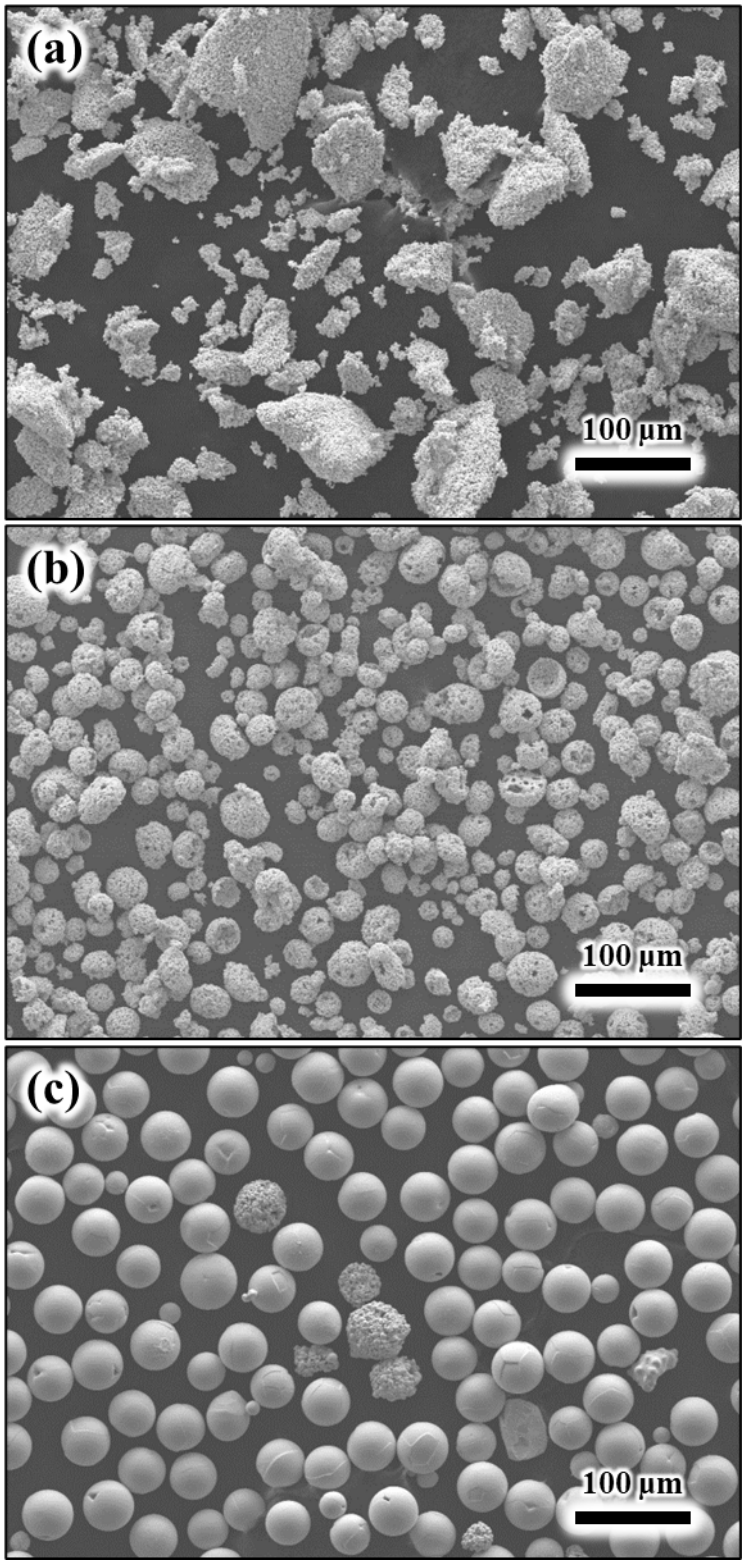

Figure 2. SEM images of (a) as-received, (b) spray-dried, and (c) plasma-spherodized pure Mo powder.

The NNSA and ORNL have invested in helping process the as-received Mo powder—whether it be pure ^{Nat}Mo or enriched aMo powder—to make it an optimal for processing for LPBF. Pure ^{Nat}Mo is not commonly found in nature as the sulfide ore, molybdenite (MoS_2). Molybdenite is typically oxidized to make MoO_3 and then purified by sublimation. The purified MoO_3 is commonly converted to metal though a twostep hydrogen reduction with the final step occurring at in the 1050 °C range. Ammonia based processing can also be used to convert MoO_3 to $(NH_4)_6Mo_7O_{24}$, otherwise known as ammonium heptamolybdate (AHM). The MoO_3 produced from AHM is first reduced under low-temperature conditions (550–750°C) due to the low melting temperature (795°C) by flowing H_2 into the furnace atmosphere, leaving behind MoO_2, which has a higher melting temperature. The MoO_2 can then be further reduced at higher temperatures (~1,100°C), leaving pure Mo. Powder agglomeration will occur during heating to high temperature. Ball milling can be employed to break up the powder produced by either method, however, the resulting particle geometry will be irregular.

Alternatively, the agglomerated powder can be processed using the Niro spray dryer shown in Figure 3(a). The agglomerated powder is usually mixed with a binder, which can be as simple as choosing a solvent such as methanol. Spray dryers are designed with an atomizer that disperses the slurry through a nozzle. Hot gas is jetted from the sides of the nozzle, which will break up the powder particles, typically leaving a spherical geometry with particle size ranges of 50–300 µm. An example of spray-dried Mo powder is shown in Figure 2(b). Although these particles are spherical, the powder size is not optimal for LPBF. Moreover, depending on the material, the particles may have a porous structure, which could hinder densification during the laser-melting process.

Figure 3. (a) The Niro spray dryer and (b) Tekna plasma spherodization systems located at ORNL.

Once the powder is no longer agglomerated, it can be spherodized with the Tekna TekNano-15 plasma spherodization system shown in Figure 3(b). The Tekna will feed powder particles one by one through a nozzle that flows into a chamber, exposing them to a plasma. During exposure to the plasma, the powder particles will melt, excess chemical species such as O or N will be carried away, and the particle will resolidify as a solid sphere because of surface tension held through the circulation of a feeder gas. The resulting morphology of Mo powder after spherodization is shown in Figure 2(c). Spherodized powder can then be fed into an LPBF system and easily processed because spherical powder is free-flowing and easily spreadable.

2.2 LASER POWDER BED FUSION

LPBF was chosen because it uses a powder feedstock, yields a high geometric resolution (<200 µm), and can be easily performed with different materials. A Renishaw AM250, shown in Figure 4(a), was chosen for the ^{99}Mo project because it comes with a reduced build volume (RBV) insert, shown in Figure 4(b). The main powder silo for the Renishaw to use its full build volume of 250 × 250 × 250 mm requires a minimum of ~2 L of powder. Using the RBV, only ~250 mL are needed to perform successful builds, which may be important for handling small batches of powder that may be costly to acquire, such as that for aMo. However, the build volume is reduced to 78 × 78 × 78 mm, but it is still large enough to fabricate the 29 mm outer diameter targets. Multiple geometries and components based on complex

designs were fabricated from pure Mo powder using the Renishaw AM250 and RBV, and a selected few are shown in Figure 4(c).

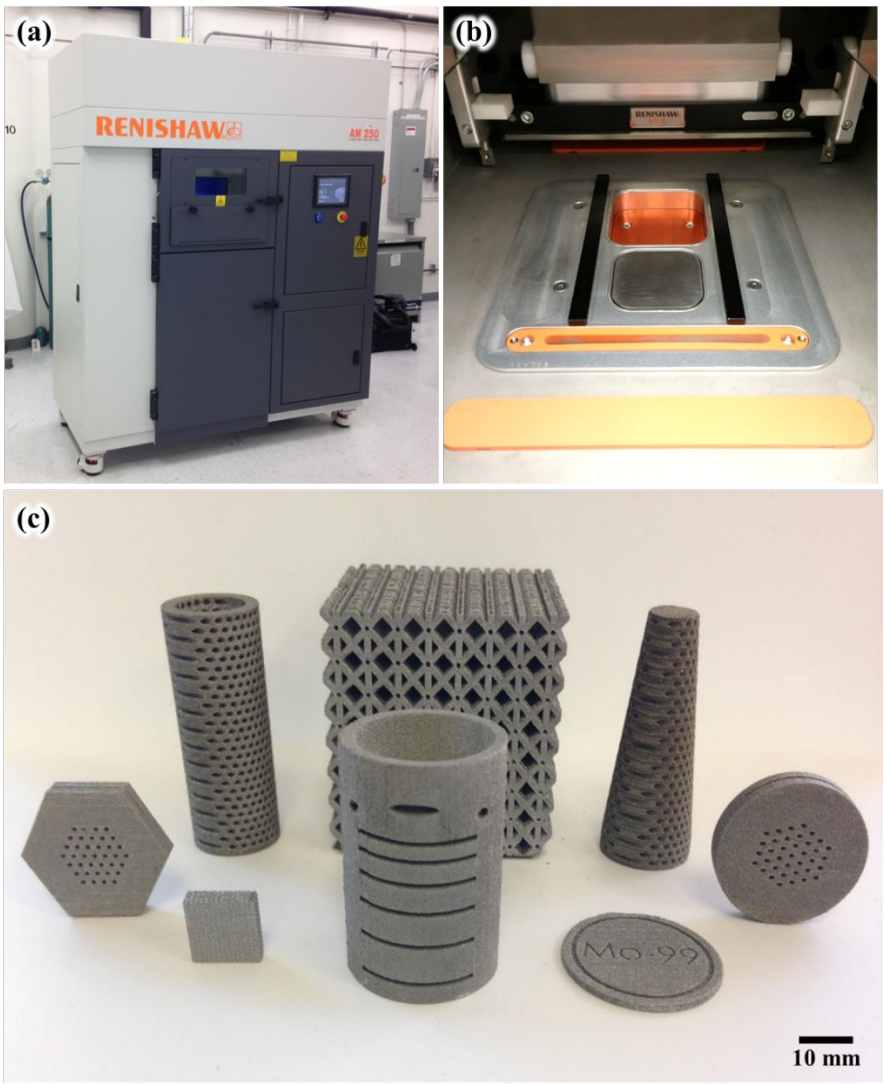

Figure 4. The (a) Renishaw AM250 LPBF system and its (b) RBV setup installed in the build chamber; (c) Different geometries printed from pure Mo powder based on design work from the Molybdenum-99 Program.

For processing of Mo or other refractories, the Renishaw AM250 was retrofitted with a 400 W Yb-fiber pulsed laser. For LPBF processing of commercial Fe- and Ni-based alloys, optimum laser powers <200 W are often used because these alloys have a low melting temperature compared with Mo. The higher laser power on this machine is expected to overcome the higher melting temperature of refractory materials. Moreover, the laser spot size of the Renishaw is ~130 µm, which was chosen over the more common ~70 µm spot size more commonly seen in commercial machines to try to reduce thermal stresses that may cause the Mo to crack.

Besides the laser source, any desired gas can be flown into the chamber to help control the solidification and build quality. Inert gases such as Ar are the most common for trying to reduce the O_2 content below 2,000 ppm. Refractory metals often have a higher affinity for O_2 at higher temperatures and therefore may

oxidize during the LPBF process when using only Ar. Therefore, a mix 2% H_2-Ar mix was found to help minimize oxidation during the building.

Many different parameters can be varied in the Renishaw, but the most common include the incoming laser power, the raster scan speed of the laser (in the case for a pulsed laser, this is represented by the jumping point distance and dwell time at each point), the distance between consecutive scans (i.e., hatch spacing), and the powder layer thickness. These parameters are often normalized with the laser energy density (ED) and expressed as:

$$\mathrm{ED} = \frac{\text{Laser Power}}{\frac{\text{Point Distance}}{\text{Dwell Time}} \times \text{Hatch Spacing} \times \text{Layer Thickness}}. \tag{1}$$

Although the ED is reliant on only five parameters, multiple variations are possible in the macro- and microstructure of the formed part. These variations can include defects such as cracks and pores, as well as anomalous grain growth, which will affect mechanical and thermal performance. Parametric studies are often performed to map out the defect evolution for a given material. Simple geometries such as cubes can be printed with multiple cubes in one build. If, for example, the cubes are built in an array such as the one shown in Figure 5(a), then one cube will be processed with all parameters held constant, except for one that can be incrementally varied between each cube in a row. Thus, multiple rows of cubes can be fabricated with varying parameters, as shown in Figure 5(b). Afterward, these cubes can be subjected to macro- and microstructural characterization.

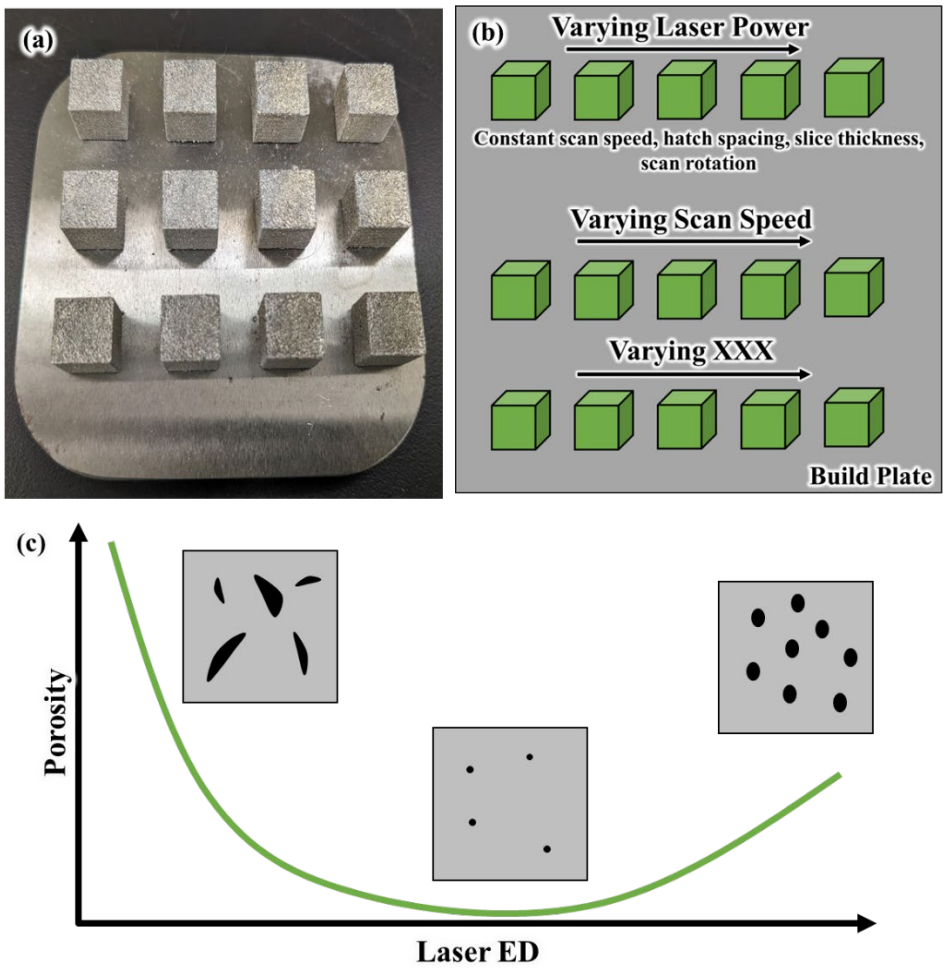

Figure 5. Examples of processing parametric studies performed by (a) printing simple cubic geometries in which (b) the LPBF parameters can be easily varied between each cube. The cubes can then be subjected to density and macrostructural investigations to map out the evolution of defects and determine where the optimum parameters near full density can be achieved.

Often, LPBF parameters with near-full density are most desired, so the density of the cube samples is measured by immersion density, x-ray tomography, optical analysis, or a pycnometer. A curve such as the one shown in Figure 5(c) can then be generated, which typically follows a common behavior in which using lower ED will result in irregular pores due to a lack of fusion [14, 15]. There will be some middle ground in laser energy in which near-full density can be achieved, but as the laser energy continues to increase past the optimum region, more keyholes will be created, and boiling of the melt will occur, producing spherical pores [14, 15].

2.3 MATERIALS CHARACTERIZATION

ORNL has a strong background in materials characterization. Multiple facilities are outfitted with light and electron microscopes, x-ray diffraction, mechanical tensile/compressive testing, and so on. Two unique capabilities acquired specifically for analyzing AM components include the Malvern Panalytical particle microscope shown in Figure 6(a) and the UES Robo-Met serial sectioning unit shown in Figure 6(b).

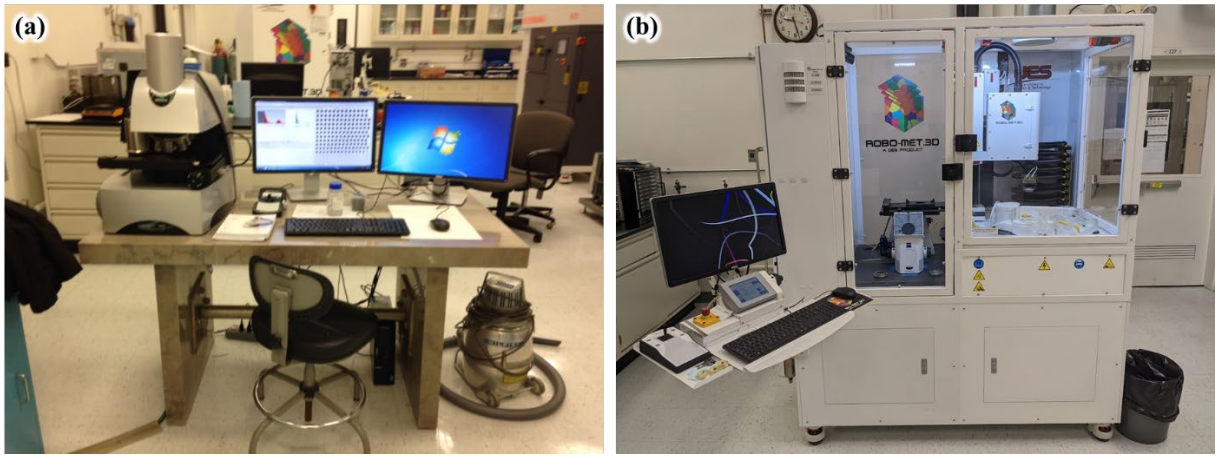

Figure 6. Characterization equipment includes (a) the Malvern Panalytical particle analyzer and (b) the UES Robo-Met serial sectioning unit.

The Malvern microscope can image and count thousands of particles per minute. Individual images are taken of each of particle to analyze the morphology and overall size. Many statistics such as average particle size distribution, average circularity, and closeness to a perfect circle can be determined.

The UES Robo-Met instrument includes a sample polishing setup on the right and a light microscope on the left. The unit has a robotic arm that can hold a mounted sample, polish it on the right side to some user specification, and subsequently image the sample. This can be performed repetitively to create a 3D profile of the sample.

3. LASER POWDER BED FUSION PROCESSING OF REFRACTORY ALLOYS

Structural materials used in the nuclear industry usually include Fe-based steels and Ni-based superalloys. Although Fe- and Ni-based alloys have high strength retention during operation at high temperatures, these structural materials could be exposed to heavy heat loads, such as the plasma in fusion reactors or radiating particles in fission reactors. Refractory metals such as Mo, Ta, and W are considered for use in armors because of their high density, high melting temperature, and good resistance to radiating particles [16-19]. Because of their high melting temperatures, refractory metals are often produced via powder metallurgy processes, such as high-temperature sintering, spark plasma sintering, and hot isostatic pressing [20]. However, producing bulk amounts of these metals remains difficult, as does machining to specific tolerances and geometric specifications. Many designs in fusion reactors often include complex shapes and bends that would be impossible to fabricate with conventional powder metallurgy processes [21, 22].

Recent progress in AM processing of metal powders has demonstrated high potential for future processing of metallic alloys toward producing customized geometries of unique design [9, 22]. In particular, LPBF is a rapid production AM process that uses a laser source to selectively melt regions of a powder bed, yielding dense, complex geometries fabricated to near-net shape [9]. Despite increasing interest and research in LPBF-processed refractory metals and alloys, it remains challenging because of the formation of defects, such as pores and cracks. Certain refractory metals—such as Nb, Mo, and Ta—have demonstrated being crack-free when processed by LPBF, except with some porosity. However, the processing window is extremely narrow, leaving little versatility for heat input variability [23, 24]. For other refractory metals, such as W, no reproducible results with crack-free parts have been reported when processed by LPBF [25-27].

Unlike W, Mo can be printed without cracks, given a certain processing window. Faidel et al. [12] was one of the first reports on the AM processing of Mo powder. Using a lower laser power of 200 W, the maximum limit of the laser used in Faidel et al. [12], the researchers printed small cubic geometries with high ED using small hatch spacings of 10 and 20 µm. The researchers also varied powder layer thickness between 25 and 45 µm over a wide scan speed range of 139 to 2,224 mm/s. The powder particle size distribution was 10–45 µm, which was within the geometric constraints of the hatch spacing and layer thickness. Choosing geometric parameters larger or smaller than the average particle size will lead to different types of defect formation. Moreover, with a low laser power of 200 W, increasing the ED required compensation from the other parameters because laser power could not be increased simply. The ED range in Faidel et al. [12] was 120–1,066 J/mm^3, whereas a typical ED for processing lower melting temperature alloys, such as Al- and Fe-based alloys, is usually <100 J/mm^3. However, the researchers observed excessive porosity in the cubic sample's cross sections, reporting nothing above 85% dense, although they did not report any cracking.

In Wang et al. [22], the authors suggested that powder quality was of the utmost importance for densification of LPBF-processed Mo. The authors acquired previously milled powder with irregular geometries that was subsequently spray-dried and plasma-spherodized (Figure 2). The resulting spherical powder appeared to be clean and free flowing but had a noticeably larger size distribution than the as-received milled powder. A Renishaw unit similar to the one in Figure 4 with a 400 W laser was used to perform the LPBF processing parametric study and focused on high EDs (i.e., 600–1,200 J/mm^3). Minimal porosity (i.e., <1%) was reported, but cracking was found in multiple samples. The authors proposed that the powder bed should be preheated to help reduce the cooling rate and avoid the ductile to brittle transition temperature of Mo which is approximately 200 °C for small grained, recrystallized Mo. Preheating was later performed in electron beam–based PBF, which resulted in near-net density and no solidification cracking [28-30].

In Bajaj et al. [31], the study showed that cracking could be eliminated with the correct processing parameters, but the authors did not report near-full density with the parameters investigated. In Braun et al. [32], the authors also reported on investigations of LPBF of pure Mo and reported that O content from the pre-alloyed powders would remain in the solidifying structure during LPBF, acting as a crack initiation site. The authors later investigated an Mo-based alloys, titanium-zirconium-molybdenum (TZM) (<1 wt % of Ti, Zr, and C in Mo) and successfully printed dense, crack-free material [33]. The authors attributed the success of printing TZM to the presence of C. Later reports showed that adding C greatly helps solidify Mo in LPBF with consistent and repeatable results [34-36].

Higashi et al. [37] and Rebesan et al. [13] revisited the solidification of Mo by LPBF, and the authors determined that microstructure was highly dependent on the LPBF processing parameters. Resulting microstructures may easily influence the crack initiation and propagation. For example, long columnar grains are often observed along the build direction in LPBF-processed parts from Al, Fe, Ni, and Ti feedstocks [38-40]. Similar cracking phenomenon have been reported in certain alloys, observing that the cracks run along the grain boundaries of these long columnar grains. Therefore, similar influences may play a role in the solidification of Mo with LPBF.

For preliminary investigations, spherical pure Mo powder was acquired from Tekna and processed with the Renishaw AM250 (Figure 4[a]) using the RBV (Figure 4[b]). Using low (200 W) and high (400 W) laser powers, the hatch spacings at each laser power were set to 40 and 80 µm, respectively, to achieve the same ED. Multiple cubic samples were processed over varying scan speeds, and an example build is shown in Figure 5(a). After printing, the samples were removed from the build plate and density-evaluated with immersion density. The resulting densities are shown in Figure 7. The lower laser power of 200 W clearly underperformed compared with the high laser power of 400 W, even though ED was kept constant. This was similar to what was first observed in Faidel et al. [12]. The highest density observed from the immersion density measurements was >98% dense.

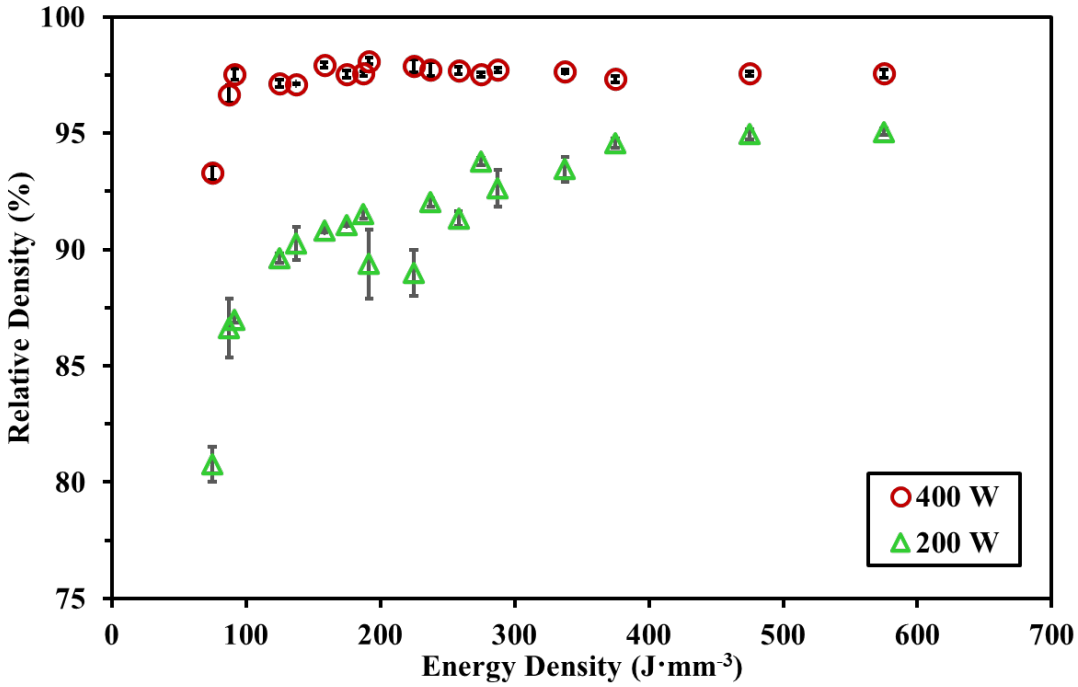

Figure 7. Density as a function of ED for pure Mo printed at low (200 W) and high (400 W) laser power.

An optical cross section image of a Mo sample is shown in Figure 8. Porosity can be minimized without solidification cracking. The parameters were not investigated thoroughly, meaning it is possible to achieve >99% density with further tailoring of the parameters. However, the authors of the present study were able to verify that Mo powder can be easily processed with LPBF on the Renishaw AM250 at ORNL. Moreover, the porosity is uniform with a high degree of open porosity that was reported to help increase the dissolution [2]. Effectively, an AM disk dissolved faster than a press and sinter disk in the same solution [2]. Subsequent builds can expand on the simple geometries and print more complex geometries relevant to the Molybdenum-99 Program, such as those shown in Figure 4(c).

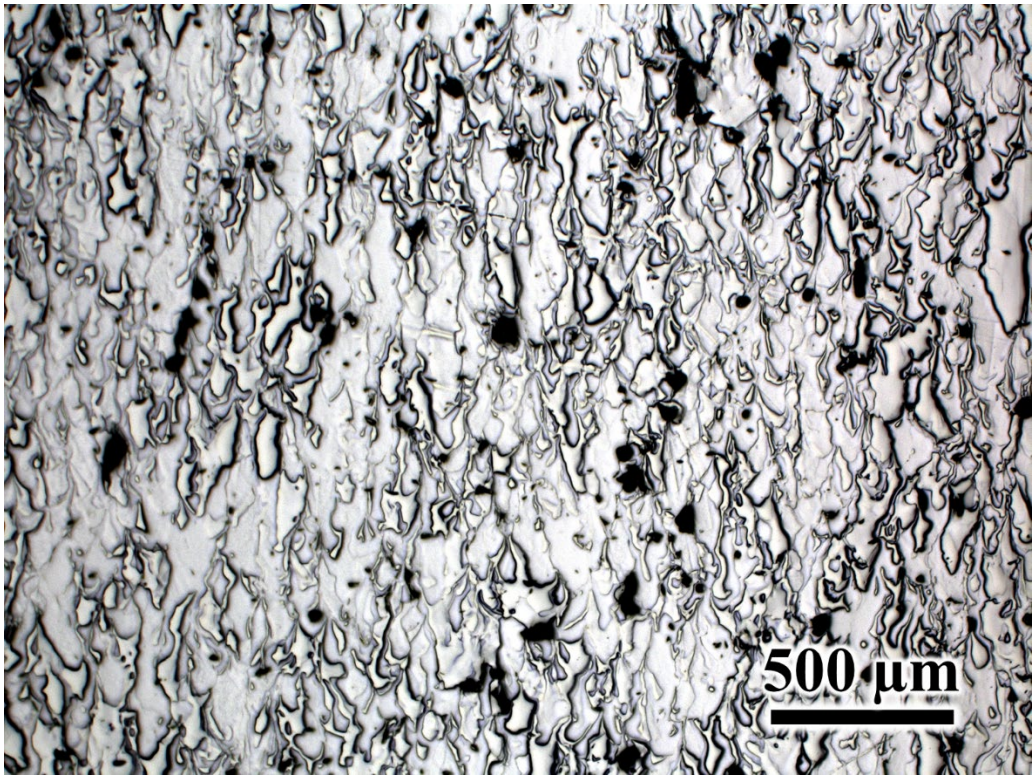

Figure 8. Optical image of the cross section of a Mo sample with respect to the build direction.

4. SUMMARY

AM processes such as LPBF can be used to fabricated custom-designed, complex components from powder feedstock. Because refractory metals have a high melting temperature, they are typically produced from a powder source via multiple processes, such as press and sinter, hot rolling, and hot extrusion. Northstar's aMo target was designed based on a disk-type geometry that can be easily and efficiently fabricated from the press and sinter method. However, because of thermal stresses that will occur once the accelerated electron beam interacts with the target, the disk might warp and could cause part failure. Therefore, if a target with a geometry optimized to handle the thermal stresses could be designed, then LPBF would be a potential route for manufacturing these complex targets. Through NNSA's Molybdenum-99 Program, significant investments were made to develop a facility at ORNL that can process pure Mo and aMo powder with emphasis on LPBF. At this AM facility, the as-received aMo powder can be processed with a spray-drying and/or plasma spherodization system to make the powders a more optimal geometry for LPBF. Subsequently, the powders can be fed into an LPBF system and easily processed with different microstructures and engineered porosity, which are critical for increased dissolution in the postprocessing steps after accelerator time. More AM and LPBF can be leveraged to produce more complex targets with more optimal geometries designed to withstand the thermos-mechanical environment in the accelerator beam.

5. REFERENCES

[1] R.A. Lowden, S. Nunn, J. Kiggans Jr, R.J. Parten, C. Bryan, "Powder Metallurgy Fabrication of Molybdenum Accelerator Target Disks", (2015), ORNL/TM-2014/238

[2] D.J. Bettinardi, P. Tkac, "Dissolution of Additively Manufactured Mo Disks and Structures for Accelerator Based Production of Mo-99", Argonne National Lab.(ANL), Argonne, IL (United States)(2020), ANL-20/48

[3] P. Tkac, G.F. Vandegrift, J. Harvey, "Dissolution of Sintered Mo Disks", Argonne National Lab.(ANL), Argonne, IL (United States)(2013), ANL/CSE-13/19

[4] K.A. Woloshun, G.E. Dale, E.R. Olivas, A.C. Naranjo, F.P. Romero, "29 Mm Diameter Test Target Design Report", Los Alamos National Lab.(LANL), Los Alamos, NM (United States)(2016), LA-UR-16-27128

[5] K.A. Woloshun, G.E. Dale, E.R. Olivas, F.P. Romero, D.A. Dalmas, S. Chemerisov, R. Gromov, R. Lowden, "Thermal Test on Target with Pressed Disks", United States, (2016), 10.2172/1245565

[6] S. Chemerisov, J. Bailey, T. Heltemes, C. Jonah, V. Makarashvili, P. Tkac, D. Rotsch, M. Virgo, G. Vandegrift, "Results of the Six-and-a-Half Day Electron-Accelerator Irradiation of Enriched Mo-100 Targets for the Production of Mo-99", Argonne National Lab.(ANL), Argonne, IL (United States)(2016),

[7] K.A. Woloshun, "Mechanical Requirements and Testing Procedure for the Target and Window", United States, (2014), 10.2172/1160095

[8] T. Debroy, H.L. Wei, J.S. Zuback, T. Mukherjee, J.W. Elmer, J.O. Milewski, A.M. Beese, A. Wilson-Heid, A. De, W. Zhang, "Additive Manufacturing of Metallic Components – Process, Structure and Properties", *Prog. Mater Sci.* 92 (2018) 112-224, 10.1016/j.pmatsci.2017.10.001

[9] W.J. Sames, F. List, S. Pannala, R.R. Dehoff, S.S. Babu, "The Metallurgy and Processing Science of Metal Additive Manufacturing", *Int. Mater. Rev.* 61(5) (2016) 315-360,

[10] H. Hyer, L. Zhou, G. Benson, B. McWilliams, K. Cho, Y. Sohn, "Additive Manufacturing of Dense We43 Mg Alloy by Laser Powder Bed Fusion", *Addit. Manuf.* 33 (2020) 101123, ARTN 101123 10.1016/j.addma.2020.101123

[11] H. Hyer, L. Zhou, A. Mehta, S. Park, T. Huynh, S.T. Song, Y.L. Bai, K. Cho, B. McWilliams, Y. Sohn, "Composition-Dependent Solidification Cracking of Aluminum-Silicon Alloys During Laser Powder Bed Fusion", *Acta Mater.* 208 (2021) 116698, ARTN 116698 10.1016/j.actamat.2021.116698

[12] D. Faidel, D. Jonas, G. Natour, W. Behr, "Investigation of the Selective Laser Melting Process with Molybdenum Powder", *Addit. Manuf.* 8 (2015) 88-94, https://doi.org/10.1016/j.addma.2015.09.002

[13] P. Rebesan, M. Ballan, M. Bonesso, A. Campagnolo, S. Corradetti, R. Dima, C. Gennari, G.A. Longo, S. Mancin, M. Manzolaro, G. Meneghetti, A. Pepato, E. Visconti, M. Vedani, "Pure Molybdenum Manufactured by Laser Powder Bed Fusion: Thermal and Mechanical Characterization at Room and High Temperature", *Addit. Manuf.* 47 (2021) 102277, https://doi.org/10.1016/j.addma.2021.102277

[14] H. Hyer, L. Zhou, S. Park, G. Gottsfritz, G. Benson, B. Tolentino, B. McWilliams, K. Cho, Y. Sohn, "Understanding the Laser Powder Bed Fusion of Alsi10mg Alloy", *Metallography Microstructure and Analysis* 9(4) (2020) 484-502, 10.1007/s13632-020-00659-w

[15] L. Zhou, H. Hyer, J. Chang, A. Mehta, T. Huynh, Y. Yang, Y. Sohn, "Microstructure, Mechanical Performance, and Corrosion Behavior of Additively Manufactured Aluminum Alloy 5083 with 0.7 and 1.0 wt% Zr Addition", *Mater. Sci. Eng. A* 823 (2021) 141679, 10.1016/j.msea.2021.141679

[16] R. Abernethy, "Predicting the Performance of Tungsten in a Fusion Environment: A Literature Review", *Mater. Sci. Technol.* 33(4) (2017) 388-399,

[17] M. Rieth, S.L. Dudarev, S.M. Gonzalez de Vicente, J. Aktaa, T. Ahlgren, S. Antusch, D.E.J. Armstrong, M. Balden, N. Baluc, M.F. Barthe, W.W. Basuki, M. Battabyal, C.S. Becquart, D. Blagoeva, H. Boldyryeva, J. Brinkmann, M. Celino, L. Ciupinski, J.B. Correia, A. De Backer, C. Domain, E. Gaganidze, C. García-Rosales, J. Gibson, M.R. Gilbert, S. Giusepponi, B. Gludovatz, H. Greuner, K. Heinola, T. Höschen, A. Hoffmann, N. Holstein, F. Koch, W. Krauss, H. Li, S. Lindig, J. Linke, C.

Linsmeier, P. López-Ruiz, H. Maier, J. Matejicek, T.P. Mishra, M. Muhammed, A. Muñoz, M. Muzyk, K. Nordlund, D. Nguyen-Manh, J. Opschoor, N. Ordás, T. Palacios, G. Pintsuk, R. Pippan, J. Reiser, J. Riesch, S.G. Roberts, L. Romaner, M. Rosiński, M. Sanchez, W. Schulmeyer, H. Traxler, A. Ureña, J.G. van der Laan, L. Veleva, S. Wahlberg, M. Walter, T. Weber, T. Weitkamp, S. Wurster, M.A. Yar, J.H. You, A. Zivelonghi, "Recent Progress in Research on Tungsten Materials for Nuclear Fusion Applications in Europe", *J. Nucl. Mater.* 432(1) (2013) 482-500, https://doi.org/10.1016/j.jnucmat.2012.08.018

[18] C. Tan, K. Zhou, W. Ma, B. Attard, P. Zhang, T. Kuang, "Selective Laser Melting of High-Performance Pure Tungsten: Parameter Design, Densification Behavior and Mechanical Properties", *Science and Technology of advanced MaTerialS* 19(1) (2018) 370-380,

[19] L. Zhou, T. Yuan, R. Li, J. Tang, G. Wang, K. Guo, "Selective Laser Melting of Pure Tantalum: Densification, Microstructure and Mechanical Behaviors", *Mater. Sci. Eng. A* 707 (2017) 443-451, 10.1016/j.msea.2017.09.083

[20] R.A. Lowden, S. Nunn, J. Kiggans Jr, R.J. Parten, C. Bryan, "Powder Metallurgy Fabrication of Molybdenum Accelerator Target Disks", *ORNL/TM-2014/238, July* (2015),

[21] S. Kanpara, S. Khirwadkar, S. Belsare, K. Bhope, R. Swamy, Y. Patil, P. Mokariya, N. Patel, T. Patel, K. Galodiya, "Fabrication of Tungsten & Tungsten Alloy and Its High Heat Load Testing for Fusion Applications", *Materials Today: Proceedings* 3(9, Part B) (2016) 3055-3063, https://doi.org/10.1016/j.matpr.2016.09.020

[22] D. Wang, C. Yu, J. Ma, W. Liu, Z. Shen, "Densification and Crack Suppression in Selective Laser Melting of Pure Molybdenum", *Mater. Des.* 129 (2017) 44-52, https://doi.org/10.1016/j.matdes.2017.04.094

[23] J. OH, T. ISHIMOTO, S.-h. SUN, T. NAKANO, "Crystallographic Texture Formation of Pure Tantalum by Selective Laser Melting Method", *Journal of Smart Processing* 8(4) (2019) 151-154,

[24] V. Livescu, C.M. Knapp, G.T. Gray, R.M. Martinez, B.M. Morrow, B.G. Ndefru, "Additively Manufactured Tantalum Microstructures", *Materialia* 1 (2018) 15-24, https://doi.org/10.1016/j.mtla.2018.06.007

[25] K. Liu, D. Gu, M. Guo, J. Sun, "Effects of Processing Parameters on Densification Behavior, Microstructure Evolution and Mechanical Properties of W–Ti Alloy Fabricated by Laser Powder Bed Fusion", *Mater. Sci. Eng. A* 829 (2022) 142177, https://doi.org/10.1016/j.msea.2021.142177

[26] B. Vrancken, R.K. Ganeriwala, M.J. Matthews, "Analysis of Laser-Induced Microcracking in Tungsten under Additive Manufacturing Conditions: Experiment and Simulation", *Acta Mater.* 194 (2020) 464-472, https://doi.org/10.1016/j.actamat.2020.04.060

[27] X. Zhou, X. Liu, D. Zhang, Z. Shen, W. Liu, "Balling Phenomena in Selective Laser Melted Tungsten", *J. Mater. Process. Technol.* 222 (2015) 33-42, https://doi.org/10.1016/j.jmatprotec.2015.02.032

[28] P. Fernandez-Zelaia, M. Kirka, Q. Campbell, J. Ortega Rojas, A. Marquez Rossy, C. Ledford, "Electron Beam Powder Bed Fusion Additive Manufacturing of Refractory Metals", Oak Ridge National Lab.(ORNL), Oak Ridge, TN (United States)(2021),

[29] P. Fernandez-Zelaia, C. Ledford, E.A.I. Ellis, Q. Campbell, A.M. Rossy, D.N. Leonard, M.M. Kirka, "Crystallographic Texture Evolution in Electron Beam Melting Additive Manufacturing of Pure Molybdenum", *Mater. Des.* 207 (2021) 109809, https://doi.org/10.1016/j.matdes.2021.109809

[30] P. Fernandez-Zelaia, C. Ledford, S. Kim, Q. Campbell, J.O. Rojas, A.M. Rossy, M. Kirka, "Mechanical Behavior of Additively Manufactured Molybdenum and Fabrication of Microtextured Composites", *JOM* 74(9) (2022) 3316-3328,

[31] P. Bajaj, J. Wright, I. Todd, E.A. Jägle, "Predictive Process Parameter Selection for Selective Laser Melting Manufacturing: Applications to High Thermal Conductivity Alloys", *Addit. Manuf.* 27 (2019) 246-258,

[32] J. Braun, L. Kaserer, J. Stajkovic, K.H. Leitz, B. Tabernig, P. Singer, P. Leibenguth, C. Gspan, H. Kestler, G. Leichtfried, "Molybdenum and Tungsten Manufactured by Selective Laser Melting: Analysis

of Defect Structure and Solidification Mechanisms", *Int. J. Refract. Met. Hard Mater.* 84 (2019) 104999, https://doi.org/10.1016/j.ijrmhm.2019.104999
[33] L. Kaserer, J. Braun, J. Stajkovic, K.H. Leitz, P. Singer, I. Letofsky-Papst, H. Kestler, G. Leichtfried, "Microstructure and Mechanical Properties of Molybdenum-Titanium-Zirconium-Carbon Alloy Tzm Processed Via Laser Powder-Bed Fusion", *Int. J. Refract. Met. Hard Mater.* 93 (2020) 105369, https://doi.org/10.1016/j.ijrmhm.2020.105369
[34] J. Braun, L. Kaserer, I. Letofsky-Papst, K.H. Leitz, H. Kestler, G. Leichtfried, "On the Role of Carbon in Molybdenum Manufactured by Laser Powder Bed Fusion", *Int. J. Refract. Met. Hard Mater.* 92 (2020) 105283, https://doi.org/10.1016/j.ijrmhm.2020.105283
[35] J. Braun, L. Kaserer, J. Stajkovic, H. Kestler, G. Leichtfried, "Grain Refinement Mechanisms of Alloying Molybdenum with Carbon Manufactured by Laser Powder Bed Fusion", *Mater. Des.* 215 (2022) 110507, https://doi.org/10.1016/j.matdes.2022.110507
[36] Y. Wu, M. Li, J. Wang, Y. Wang, X. An, H. Fu, H. Zhang, X. Yang, Q. Zou, "Powder-Bed-Fusion Additive Manufacturing of Molybdenum: Process Simulation, Optimization, and Property Prediction", *Addit. Manuf.* 58 (2022) 103069, https://doi.org/10.1016/j.addma.2022.103069
[37] M. Higashi, T. Ozaki, "Selective Laser Melting of Pure Molybdenum: Evolution of Defect and Crystallographic Texture with Process Parameters", *Mater. Des.* 191 (2020) 108588,
[38] D. Herzog, V. Seyda, E. Wycisk, C. Emmelmann, "Additive Manufacturing of Metals", *Acta Mater.* 117 (2016) 371-392,
[39] W. King, A. Anderson, R. Ferencz, N. Hodge, C. Kamath, S. Khairallah, A. Rubenchik, "Laser Powder Bed Fusion Additive Manufacturing of Metals; Physics, Computational, and Materials Challenges", *Appl. Phys. Rev.* 2(4) (2015) 041304,
[40] T.D. Ngo, A. Kashani, G. Imbalzano, K.T. Nguyen, D. Hui, "Additive Manufacturing (3d Printing): A Review of Materials, Methods, Applications and Challenges", *Composites Part B: Engineering* 143 (2018) 172-196,